# Dynamic Range-based Intensity Normalization for Airborne, Discrete Return Lidar Data of Forest Canopies

**Demetrios Gatziolis**

## Abstract

*A novel approach for improving the consistency of intensity measurements using range-based normalization is introduced. The normalization is data-driven, can be fully automated, and involves scaling differences in observed intensity between returns collocated in space but registered to different laser scanning swaths. The scaling is proportional to the overall rate of attenuation f of laser energy. The utility of this approach for applications of lidar over forests was evaluated by examining classification results of broad cover types obtained using observed and normalized intensity measurements in an Oregon study area. The normalization was more effective for single returns, leading to a 53 percent reduction in intensity coefficient of variation between observed and range-normalized measurements. The poor cover type classification accuracy (44.4 percent; kappa 0.167) obtained by using observed intensities of first returns improved substantially to 75.6 percent (kappa 0.624) when using above-ground, single returns and f = 2.04.*

## Introduction

Airborne lidar technology has been increasingly used for forestry and environmental applications (Goodwin *et al.*, 2006). In its discrete-return form, lidar generates point (often known as return or echo) cloud data precisely georeferenced in space. The information content of the lidar data and its utility for forestry applications has been exploited using primarily the three-dimensional nature of the return cloud, and only recently has intensity, an attribute of individual returns, been explored. Intensity is the only parameter of lidar data that is directly associated with surface reflectivity of illuminated objects, and hence, has target discrimination potential. The surge of interest in intensity as an information source experienced recently has been attributed to improved consistency (reduction of noise) in intensity measurements by modern lidar instruments (Korpela, 2008). Intensity has been used to separate ground from above-ground returns (Vosselman, 2000), classify lidar-derived objects (Axelsson, 1999) and tree species (Kim *et al.*, 2009), as a component of land classification or segmentation models (Brennan and Webster, 2006; Antonarakis *et al.*, 2008), to model fractional forest cover (Hopkinson and Chasmer, 2009), and map understory lichens (Korpela, 2008).

Discrete-return lidar systems emit pulses of light that illuminate targeted objects and record the portion of the pulse energy backscattered to the instrument's sensor. In a process known as pulse discretization or digitization, returns are identified as the locus of maxima in backscattered energy along the pulse trajectory. Intensity is defined as the maximum amplitude of energy received by the instrument's sensor pertaining to an individual return, and it is a quantity analogous to backscatter. Most modern systems can identify and register intensity measurements for up to four returns per pulse.

Of the laser power (amount of energy per unit time) transmitted per pulse, a portion is lost as the pulse travels through the atmosphere to the target and back. The intensity values observed are also affected by fading, which sometimes is known as speckle effect, electronic noise in the sensor or from background reflections, sensor gain (sensitivity) adjustments, the wavelength of the pulse, and the surface geometry and reflectance regime of the target. Assuming homogeneous atmospheric conditions at data acquisition time, power loss due to atmospheric attenuation proportional to the instrument-target distance (range) should be expected. Range variability is present even within a single scan line as targets at nadir are closer than those near the edge of the scan line, but its magnitude is small. For example, at a 10° scan angle and 1,000 m flight height above target, the range is only 1.5 percent longer than at nadir. Larger range variability is observed with varying platform altitude or in the presence of rugged terrain causing brighter returns (higher intensity) at ridges and dimmer returns (lower intensity) at valley bottoms (Luzum *et al.*, 2004).

A less evident implication of range variability is its effect on the distribution of returns from vegetation along the pulse trajectory. Over forested areas and at longer range, reduced pulse power due to higher atmospheric attenuation would typically generate a smaller number and proportion of intermediate returns (Hopkinson, 2007) and a higher proportion of single returns, mostly near the top of tree crowns (Goodwin *et al.*, 2006), compared to those generated from shorter range pulses. Differences in the reflectance properties of vegetation material along the vertical profile of a tree crown may increase or reduce intensity discrepancies caused by variability in range and alter the value and variance of computed intensity measurements.

The observed intensity is related to the power received by the sensor which can be expressed as (Wagner *et al.*, 2006):

USDA Forest Service, PNW Research Station, Portland, Oregon (dgatziolis@fs.fed.us).

Photogrammetric Engineering & Remote Sensing
Vol. 77, No. 3, March 2011, pp. 251–259.

0099-1112/11/7703–0251/$3.00/0

$$P_r = \frac{P_t D_r^2}{R^f \beta_t^2 \Omega} \rho A_s \quad (1)$$

where $P_r$ and $P_t$ are the received and transmitted pulse power (energy per unit time), $D_r$ is the sensor aperture size, $R$ is the range to the target, $\beta_t$ is the beam (pulse) divergence, $\Omega$ is a function of the bidirectional properties, $\rho$ is the reflectivity of the target surface, and $A_s$ is the area of the target illuminated by the pulse. For Lambertian, diffuse-reflectance surfaces, the bidirectional effects can be approximated by the cosine of the angle of incidence $\alpha$ (Hölfe and Pfeifer, 2007), which is defined as the angle formed between the normal to the surface and the trajectory of the pulse. The value of $f$ reportedly depends on the surface type of the target; a value of 2 is suggested for homogeneous targets filling the full pulse footprint, 3 for linear objects (e.g., power line wires), and 4 for individual large scatterers. $D_r$ and $\beta_t$ typically remain constant during data acquisition. Assuming the attitude and location of the airborne platform is recorded during the flight, $A_s$, $\alpha$, and $R$ can be computed for every return. Because $P_t$ is subject to random but rarely-recorded variation introduced by the scanner's electronics, $P_t$ remains a target-independent source of variability in intensity measurements while $\rho$ offers target-dependent contributions to the observed intensity.

Of all parameters in Equation 1, the range to target $R$ is considered the most important factor to be accounted for with intensity data from vegetation surfaces (Hopkinsson, 2007; Kaasalainen *et al.*, 2007). Range-normalized intensity $I_{norm}$ is computed as:

$$I_{norm} = I_{obs}\left(\frac{R_{act}}{R_{ref}}\right)^f \quad (2)$$

where $I_{obs}$ is the observed intensity, $R_{act}$ is the actual distance between the laser instrument and the return, $R_{ref}$ is a reference distance either determined as a moment, usually the mean, of the distribution of $R_{act}$ from all returns or it is specified arbitrarily by the user, and exponent $f$ represents the rate of energy attenuation sustained by the pulse as it travels through a medium to and back from a target. In acquisitions over flat or rolling terrain the effect of range variability on observed intensities is likely negligible, at least as long as $f$ is within the lower half of its theoretical range. In such terrain conditions, Ahokas *et al.* (2006) achieved absolute intensity normalization and managed to retrieve precise reflectance values of flat brightness panels from intensity data using $f = 2$, as did Hopkinson (2007) in analysis of factors that affect the observed intensity distribution in vegetated environments. Using predefined, homogeneous targets scanned from multiple flight heights and $f = 2$, Hölfe and Pfeifer (2007) estimated using least squares adjustment the parameters of an empirical, global correction function with which they achieved a 70 percent reduction in the coefficient of variation (CV) of the observed intensities. They obtained similar results using an alternative, mathematical model based on the physical principle of radar systems. Korpela (2008), however, noted that the optimal value of $f$ varied from 2.3 to 2.5 for surfaces consisting of shrubs, lichens, grass, or gravel. Recently, Korpela *et al.* (2010) examined the relationship between $f$ and the intensity CV in canopy returns for thousands of trees belonging to several different species and investigated the effects $f$ had on species classification performed using 13 intensity-derived variables. It was determined that the values of $f$ minimizing the CV were higher for conifers than for hardwood species and lower for single returns compared to first or all returns for all species, and that using post-normalized intensities improved the classification results only slightly (2 to 3 percent). The values of $f$ minimizing the intensity CV by species differed from those maximizing classification accuracy, a fact attributed to the low variability of range within the study area.

The large distance deviations between laser instruments and targets often observed in acquisitions over steep terrain characterized by alternating ridges and valleys, or where platform altitude varies considerably, lead to $R_{act}$ / $R_{ref}$ ratio values (Equation 2) well outside the 0.9 to 1.1 range for a large proportion of returns. In such circumstances, failure to properly adjust the value of parameter $f$ used during normalization will likely fall short of completely removing range-induced variability in intensity measurements. To date, there is little information available on how to optimize range-based normalization of lidar intensity in different biomes and terrain conditions. This study introduces (a) a novel approach which enables dynamic (laser data driven) intensity normalization of discrete laser data, and (b) an evaluation of the effects of the normalization on intensity-based classification of forest cover type. The investigation is performed using lidar data from the temperate rainforest of Western Oregon and concurrent field data from 45 plots.

## Methods

### Study Area

The 9,500 ha study area is located in Lincoln County in the state of Oregon, approximately 30 km inland from the Pacific Ocean (Figure 1), and centered at 44° 32′N, 123° 39′W. More than 90 percent of the area is temperate rainforest, with 2,000 mm mean annual precipitation. Nearly half of the forests are privately owned and managed primarily for commercial timber. Prevalent species include Douglas-fir (*Pseudotsuga menziesii* (Mirb.) Franco), bigleaf maple (*Acer macrophyllum* Purgh), and red alder (*Alnus rubra* Bong.), with the hardwoods usually occupying buffer zones around

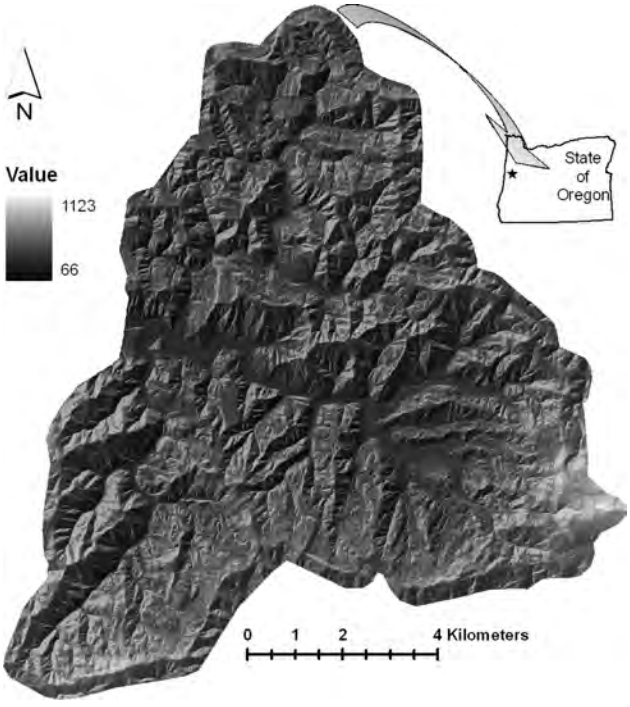


Figure 1. Study area.

the drainage network. Excluding recently-planted or thinned stands, typical forest canopy cover exceeds 90 percent. The mean and 75$^{th}$ percentile of vegetation height are 22.6 m and 30.3 m, respectively. Elevation ranges from 66 to 1,123 m above sea level and terrain is characterized by steep slopes. Over the forest area the mean slope is 61 percent, and the 75$^{th}$ slope percentile is 84.

#### Field Data

Forty five fixed-area plots of 15 m radius were established in the study area in the summer of 2005 distributed across classes of cover type (conifers, hardwoods, and mixed), tree size, and stand density. On each plot, all trees with diameter at breast height (DBH) exceeding 12.7 cm, or of dominant or co-dominant status regardless of DBH, were tallied, and their stem position was referenced using tape and compass relative to the plot center. For each tree, the species and DBH were recorded, and the projection of its crown to the ground was delineated using distance and azimuth measurements from the center of the tree stem. Where possible, plot centers were georefenced precisely by way of kinematic GPS; otherwise, by using transects surveyed with a theodolite from reference locations in forest openings. Plots were assigned to cover type according to the within-plot crown area of conifer or hardwood trees tallied. Plots with total crown area for both coniferous and hardwood species exceeding 20 percent were characterized as "mixed." Twenty plots were classified as coniferous, 11 as mixed, and 14 as hardwoods. The plot assignment to cover type did not change when alternative classification criteria were used (percent basal area or volume).

#### Lidar Data

Lidar data were acquired at leaf-on conditions in July 2005 using an aircraft-mounted Optech 3100 system from a mean height of 1,000 m above ground. The lidar instrument transmitted near-infrared light at 1,064 nm, operated on a 71 kHz repetition rate, had nominal spot spacing and footprint diameter of 0.32 m and 0.33 m, respectively, 28° scan width, 5° forward scan angle, and 50 percent or higher sidelap between adjacent scanning swaths. This configuration yielded a mean density of 7.52 returns per square meter. Returns with scan angle higher than 10° from nadir were eliminated by the data vendor prior to data delivery. Intensity was recorded as a 10-bit integer (value range 1 to 1,024) and later converted to 8-bit resolution (value range 1 to 255) by truncation of values larger than 255 that affected less than 0.01 percent of all returns. Pulse discretization enforced a minimum of 3 m between a first and a second return and 2 m between subsequent returns along the pulse trajectory. Sensor location and aircraft attitude vectors were recorded at 5 Hz. The laser data were delivered by the vendor in binary format (LAS 1.1) included pulse transmission time stamp, and were organized in 1 km$^2$ tiles.

Digital terrain (bare-ground) models (DTMs) of 1 m resolution and co-registered vegetation surface rasters were generated using the methodology described in Chen (2007). Vegetation height rasters were generated by subtracting the DTMs from the vegetation surface rasters. The location of the sensor, necessary for the computation of $R_{act}$ for every return, was linearly interpolated between the two nearest (in time) aircraft trajectory positions identified by using the time stamp of the return's parent pulse. The range for each return, $R_{act}$, was computed as the Euclidean distance in three dimensions to the sensor. $R_{act}$ was split into atmospheric and canopy components computed considering the trajectory of the return's parent pulse and the vegetation surface rasters.

#### Intensity Normalization and Plot Classification

A preliminary assessment of range-based intensity normalization effects was performed by visually examining 5 m, mean intensity rasters generated using single and first-of-many returns. In the presence of vegetation, only returns positioned in the upper 2 m of the canopy were included in the computations (Figure 2). Mean intensity rasters were generated for $f = 0$ (observed intensity), 2.0, 2.5, and 3.0 using Equation 2. As expected, higher mean intensities, depicted in lighter tone in Figure 2, corresponded well with ridges due to the short return range effective there, and individual scanning swaths could be easily discerned. The raster generated by using $f = 2.0$ (Figure 2b) still exhibited terrain and scanning swath patterns but less pronounced compared to those in the observed mean intensity raster (Figure 2a). Intensity patterns evident when using $f = 3$ (Figure 2d) appeared reversed compared to those of $f = 2$, indicating range overcompensation, especially along the terrain ridge shown at the northern half of Figure 2e. Using $f = 2.5$ (Figure 3c) yielded a raster practically free from obvious terrain elevation patterns although portions of certain scanning swaths could still be detected. Examining mean intensity rasters generated using finer increments of $f$ between 2.2 and 2.5 revealed virtually no visually discernible differences between them. These observations raised concerns that attempts to determine the optimal value of $f$ through visualization of intensity-derived rasters would likely produce subjective results. It also emphasized the need for establishing a quantitative criterion capable of determining the optimal value of $f$ dynamically, and hence of potential to be applicable to any forest application of lidar data. The minimization of post-normalized intensity variance is a reasonable criterion, but its practical application requires that the returns are constrained within a predetermined area. Otherwise, a global minimization, apart from being computationally challenging for large acquisitions, would be influenced more by the composition of targets in the entire acquisition area and their backscattering properties and less by the variability in return range. Constraining the optimization within a two-dimensional "moving" window would require predetermining the proper window size, an often non-trivial task, and would not guarantee adequate range variability within the window which is a prerequisite for the minimization of variance in observed intensity (Hölfe and Pfeifer, 2007). In the Korpela *et al.* (2010) study, ancillary information (crown delineations of individual trees) was used to spatially constrain the extent of returns included in the computation of $f$ that minimized the post-normalized intensity CV.

In this study the optimal value of exponent $f$ was derived by exploiting the data redundancy present in the overlapping portions of adjacent scanning swaths. Initially, pairs of returns positioned within a small distance from each other in three dimensions were identified, with the provision that each return in a pair belongs to a different scanning swath. In acquisitions performed using larger scan angles (>15°), the formation of pairs can be further constrained by specifying a predetermined minimum in the difference of angle of incidence between two returns. Either of these two provisions increases the probability of higher range variability within paired returns. The latter provision was not exercised in this study because scan-angle filtering of individual returns by the data vendor led to a narrow distribution of $\alpha$ values (95$^{th}$ percentile = 9.16°, $cos = 0.987$), and therefore a negligible influence of $\alpha$ on the observed intensities. The value of $f$ was computed as the one that minimized the root mean square differences (RMSD) of paired, range-normalized intensities or:

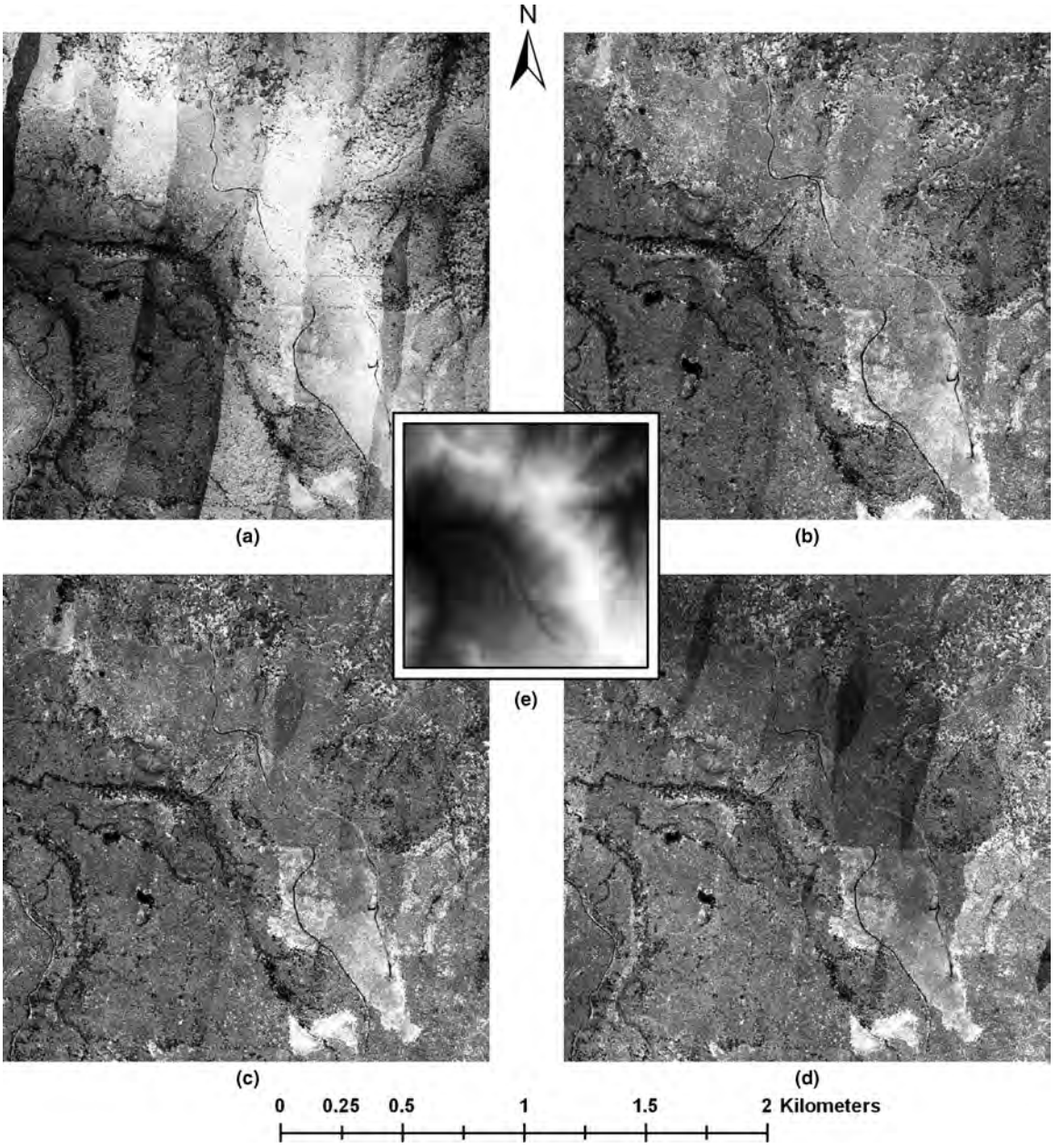


Figure 2. Range-based intensity normalization rasters: (a) original intensity ( $f = 0$), (b) $f = 2$, (c) $f = 2.5$, and (d) $f = 3$ for various values of range-scaling exponent $f$ and study area DEM (e). Raster cell values, recorded in 8-bit, were computed using the mean intensity of above ground first of many or single returns. Darker / lighter tones indicate lower / higher mean intensity or DEM elevation. Rasters are shown without any contrast enhancements.

$$\sqrt{\frac{\sum_{i}^{N}(I_{i1}\left(\frac{R_{i1}}{\overline{R}}\right)^{f} - I_{i2}\left(\frac{R_{i2}}{\overline{R}}\right)^{f})^{2}}{N}} \tag{3}$$

where $N$ is the number of return pairs identified, $I_{i1}$ and $I_{i2}$ are the observed intensities of the earlier and later acquired return in a pair, $R_{i1}$ and $R_{i2}$ are the corresponding ranges, and $\overline{R}$ is the mean range across all paired returns. Because these practically collocated returns represent energy backscattered from the same object surface, a major part of any discrepancy in their $I_{obs}$ would be indicative of differences in $R_{act}$. Optimal $f$, the one that minimizes Equation 3, can be determined using an iterative process. Computations can be expedited due to the fact that the RMSD of paired intensities was found to have a quadratic relationship to $f$, and therefore a single minimum. A golden section search routine (Press *et al.*, 2002) was used to efficiently determine $f$ from Equation 3.

The distance threshold used to identify return pairs was set to 16 cm, almost half the nominal pulse footprint diameter. The magnitude of the distance threshold ensured

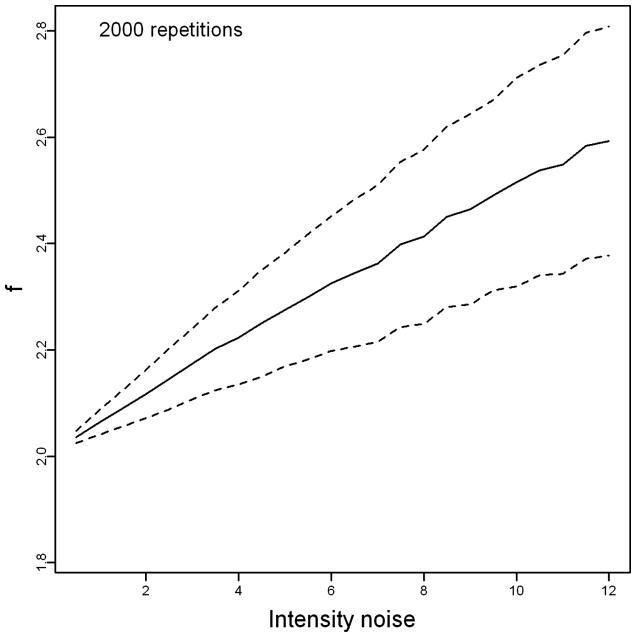


Figure 3. Mean (solid line) and standard deviation envelope (dash lines) of intensity range-scaling exponent *f*, computed using simulation that added increasingly higher amounts of noise to the observed intensity of paired returns from grass fields.

adequate spatial overlap between the footprints of the parent pulses of paired returns. To obtain a baseline estimate of *f* values over a homogeneous vegetation target, the intensity normalization approach introduced here was first employed with returns from flat fields in the middle of the study area covered with short grass. Dependence of *f* on return type was investigated by computing its optimal value separately for each return- and pulse type-specific data subsets or type combinations. The sensitivity of *f* to progressively larger amounts of noise added by means of simulation to observed intensity measurements was also investigated. All calculations were enabled by custom scripts written in the C programming language.

Plots were assigned to coniferous, mixed, or hardwood classes by using the linear discriminant function described in Venables and Ripley (2002) with equal prior class probabilities. By considering the mean and variance of the class attribute, in this case intensity, the univariate implementation of the function partitions the potential range of intensity values into class-labeled segments which are then used to assign independent observations to a particular class. Several classification trials were evaluated using cross validation for a variety of return- and pulse-type laser data subsets. Accuracy assessment was based on the percent of correctly classified plots and the confusion matrix kappa measure (Cohen, 1960), and significance between classifications was determined by computing the Z score of corresponding kappa's (Rosenfield and Fitzpatrick-Lins, 1986; Hudson and Ramm, 1987).

## Results

The mean range and standard deviation of paired, above-ground vegetation returns across all flight lines were 1,004.06 m and 137.95 m, respectively. The range for every one in three returns (33.5 percent) deviated from the mean range across all above-ground returns by more than 10 percent. The range of returns in the 45 plots varied between 45 and 215 m, with a mean of about 131 m.

In grass fields, where owing to the discretization rules, only single returns were present, the normalization procedure yielded 35,426 pairs with mean range 1,051 m and optimal $f = 2.002$. The observed and post-normalized mean intensity for all pairs were 89.6 and 88.8, respectively, and the corresponding intensity RMSD was reduced from 25.168 before to 6.136 after normalization, resulting in a 75.4 percent reduction in intensity CV. Adding random noise drawn from uniform $[0,k]$ distributions to observed intensities using simulation with 2,000 repetitions, led to a linear increase in the value of optimal *f* and inflation of its variance with progressively larger *k* values (Figure 3).

Optimal *f* was found to be return- and pulse-type specific. Considering above-ground, vegetation return pairs yielded $f = 2.042$ for single returns, 2.338 for first of two, and >2.600 for first of three or four returns. The *f* value varied between 2.400 and 2.600 for all 2nd, 3rd, and 4th returns (Table 1). As indicated by computed within-canopy ranges, pairs of single returns were positioned higher in the canopy (had shorter overall range) and had higher mean intensities compared to first of many return pairs. The improvement in the consistency of between-pair intensity (reduction in CV) achieved by range normalization did not exceed 13 percent for all 2nd to 4th returns (Table 1) but was substantial for single returns. For those returns, a strong relationship ($R^2 > 0.99$) was identified between the value of optimal *f* and the within-canopy distance from the canopy surface to the return along the parent pulse's trajectory (Figure 4). The value of *f* was found to increase linearly for single returns located no lower than 10 m from the canopy surface and to reach an asymptote for returns 20 m or more below the canopy surface.

The histogram of normalized intensity differences for pairs of single, above-ground returns was far more leptokurtic than the corresponding distribution of the observed differences, with few within-pair absolute intensity differences larger than 25 units (10 percent of the nominal intensity range) (Figure 5). Comparatively, absolute differences larger than 25 units were still frequent in histograms computed using both single and 1st returns. Similarly constructed histograms for all 2nd, 3rd, or 4th returns, and for all returns in 2-, 3-, or 4-return pulses differed very little. For those returns, the reduction in intensity CV achieved by the normalization and reported in Table 1, stems from lower return frequencies near the histogram tails.

The improved consistency in intensity achieved by the normalization process propagated through the computation of cover-type signatures and metrics to ultimately improve classification accuracy. Not surprisingly, return types that exhibited the highest reduction in intensity CV yielded the best cover type classification accuracies, while classifications based on observed intensities had poor accuracy, with kappa always below 0.2 (Table 2). Normalization of first and single returns with optimal $f = 2.326$ lead to 28 out of 45 plots assigned to the correct class with kappa = 0.426. Class-conditional kappa was lower for mixed plots. Performing the normalization for first and single returns with the alternative *f* values used for the initial visual assessment of intensity rasters (Figure 2) yielded higher intensity CVs across cover type classes, less compact, higher-variance class signatures, and classification accuracies inferior to those obtained when using $f = 2.326$. Using single returns and optimal $f = 2.042$, yielded the highest accuracy with 34 plots correctly classified, a gain of 6 plots compared to the previous case, and kappa = 0.624. Using the standard value of *f* (2.000) suggested in other studies with single returns, led to a small reduction in the percent of correctly classified plots and the corresponding kappa values,

TABLE 1. STATISTICS AND DISTRIBUTION MOMENTS OF OBSERVED AND RANGE-NORMALIZED INTENSITIES OF ABOVE-GROUND, PAIRED RETURNS FOR COMBINATIONS OF RETURN AND PULSE TYPES

| | | Number of returns in parent pulse | | | | | | Number of returns in parent pulse | | |
|---|---|---|---|---|---|---|---|---|---|---|
| | | 1 | 2 | 3 | 4 | All | | 3 | 4 | All |
| $\overline{R_{can}}$(m) | 1st returns | 4.9 | 7.2 | 8.4 | 9.9 | 6.4 | 3rd returns | 27.2 | 25.5 | 23.3 |
| $pre\bar{I}$ | | 78.3 | 48.9 | 25.7 | 16.5 | 55.0 | | 14.1 | 11.5 | 13.3 |
| $post\bar{I}$ | | 75.4 | 47.6 | 25.6 | 16.3 | 53.7 | | 13.9 | 10.9 | 12.8 |
| $f$ | | 2.042 | 2.338 | 2.613 | 2.632 | 2.326 | | 2.486 | 2.465 | 2.477 |
| $\Delta R$(m) | | 134.5 | 136.4 | 134.3 | 137.1 | 136.1 | | 140.3 | 134.8 | 138.2 |
| $preRMSD(I)$ | | 29.6 | 32.4 | 25.3 | 17.6 | 31.9 | | 20.4 | 15.2 | 19.3 |
| $postRMSD(I)$ | | 13.4 | 25.0 | 20.8 | 14.6 | 22.4 | | 18.2 | 12.9 | 16.9 |
| $\%\Delta CV_I$ | | 53.0 | 20.7 | 17.3 | 16.1 | 31.2 | | 9.5 | 10.2 | 9.0 |
| $N_{pairs}(x10^5)$ | | 6.882 | 6.296 | 2.301 | 0.352 | 28.036 | | 0.442 | 0.528 | |
| $\overline{R_{can}}$(m) | 2nd returns | | 21.4 | 16.4 | 17.3 | 18.6 | 4th returns | | 31.8 | |
| $pre\bar{I}$ | | | 24.9 | 18.5 | 14.9 | 22.2 | | | 10.7 | |
| $post\bar{I}$ | | | 23.6 | 17.3 | 13.9 | 20.9 | | | 10.4 | |
| $f$ | | | 2.402 | 2.574 | 2.587 | 2.484 | | | 2.454 | |
| $\Delta R$(m) | | | 136.6 | 132.3 | 136.4 | 134.1 | | | 140.9 | |
| $preRMSD(I)$ | | | 30.9 | 20.6 | 16.3 | 26.3 | | | 15.1 | |
| $postRMSD(I)$ | | | 25.4 | 16.8 | 13.2 | 21.5 | | | 13.4 | |
| $\%\Delta CV_I$ | | | 13.2 | 13.2 | 13.3 | 13.3 | | | 8.7 | |
| $N_{pairs}(x10^5)$ | | | 6.576 | 4.497 | 0.724 | 17.958 | | | 0.098 | |

$\overline{R_{can}}$: Mean, within-canopy range; $pre\bar{I}$ : Mean observed intensity; $post\bar{I}$ : Mean normalized intensity; $f$: exponent of range-scaling factor; $\Delta R$: root mean square difference of within-pair ranges; $preRMSD(I)$: Observed, within-pair,root mean square intensity difference; $postRMSD(I)$: normalized, within-pair, root mean square intensity difference; $\%\Delta CV_I$: percent reduction in intensity coefficient of variation between observed and range-normalized intensities; $N_{pairs}$: Number of identified return pairs.

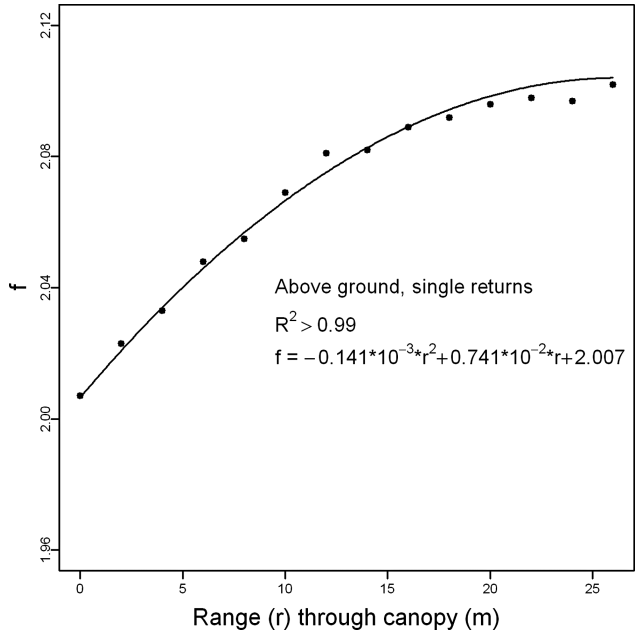


Figure 4. Relationship between intensity range-scaling exponent $f$ and within-canopy range for above-ground, single returns and fitted second-order polynomial function.

but was shown to improve the conditional kappa for conifers to 0.700, while for hardwoods conditional kappa dropped to 0.598. All other return-type combinations offered a marginal improvement to classification accuracy compared to that obtained by using observed intensities. Classification results obtained by using single returns normalized with either $f = 2.000$ or $f = 2.042$ were significantly better at 5 percent confidence level than those obtained by using first and single returns and $f$ between 2.000 and 3.000, and significantly better at 1 percent confidence level from those obtained by using observed intensities (Table 3). Classification results obtained by normalizing single returns using the standard value or 2.042 for $f$, or single and first returns and $f$ between 2.000 and 3.000, were not significantly different.

Range-normalization results were robust against the number of return pairs used to obtain them, provided that pairs were proportionally distributed to range classes and scanning swaths. Optimal $f$ computed using 100, 50, 25, and 10 percent of all return pairs differed by less than 0.042. This finding indicates that the normalization process can be expedited by limiting the identification of return pairs to a strategically selected small number of scanning swaths, or parts of swaths.

## Discussion

The findings of this study offer interesting insights into how laser pulse energy interacts with non-opaque objects such as forest canopies. The study by Kaasalainen *et al.* (2007) corroborated that $f = 2.000$ provides the correct amount of intensity scaling to compensate for range differences. A common justification for using this standard value is that it conforms to the dimensionality and reflectance properties of the majority of target surfaces, including vegetation. An alternative interpretation offered here shifts focus from the reflectance regime or backscattering properties of target surfaces to energy attenuation rates that laser pulses sustain along their trajectory. Excluding conditions characterized by extreme vapor content or concentration of pollutants, the rate

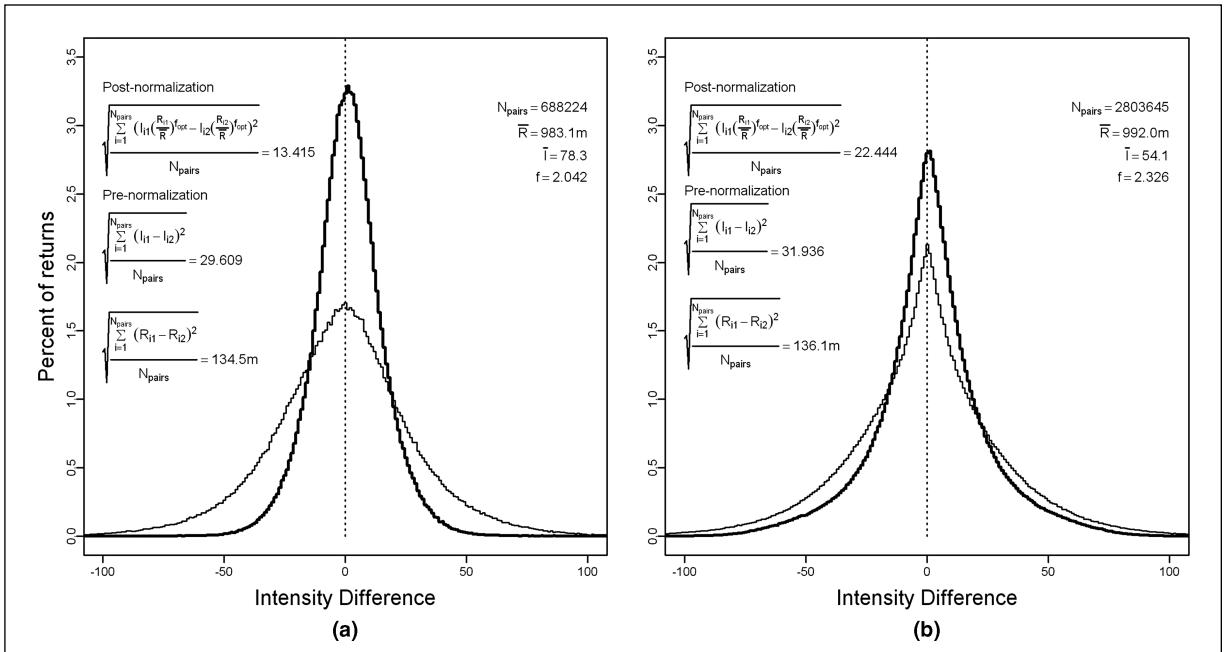


Figure 5. Distribution of pre- (thin lines) and post-normalized (thick lines) intensity differences of within vegetation, above-ground return pairs for (a) single returns, and (b) first of many or single returns.

of attenuation through the atmosphere is precisely the one computed by using $f = 2.000$. The experimentation with the intensity of returns from short grass (Figure 3) shows that the consistency of post-normalized intensity is maximized with an $f$ value that is almost identical (2.002) to the standard value, although the reflectance properties of grass do not approximate those of reflectance panels. Similarly, single returns near the top of the forest canopy yielded $f$ values that are less than 1 percent different than the standard. Their pulse energy had to penetrate almost 20 m into the canopy before a 5 percent increase in the value of $f$ (2.100) relative to the standard could be registered. This indicates that the within-canopy attenuation rate along the trajectory of single-return pulses is higher that the atmospheric attenuation but low enough not to trigger a weak, first of many returns. Single returns are generated where nearly unobstructed pulse energy that has already traveled a certain distance within canopy suddenly reaches a strong backscatterer which depletes the pulse from most of its energy and nullifies the probability of a second return. Hence the locus of a single return can be thought of as coinciding with an abrupt transition from low to very high attenuation rate. It could therefore be argued that the value of parameter $f$ computed by using single returns represents collectively the standard atmospheric plus a low canopy attenuation rate and not the backscattering properties of the object surface at the return's locus, as it has been commonly suggested in other studies. It should be noted that the affiliation between observed laser intensity and energy attenuation rates proposed here is limited to the value of parameter $f$, not the actual intensity measurements.

Table 2. Cover Type Class Signatures and Accuracy Assessment Measures of Lidar Iintensity-based Cover Type Classification for Selected Types of Above Ground Returns from 45 Plots Before and After Rrange-based Normalization; $f$ Denotes the Exponent of Range-scaling Used in the Normalization Process

| | | | Intensity class signature moments Mean (st.dev.) | | | Intensity CV (all | Classification accuracy Percent correctly | kappa | | | |
|---|---|---|---|---|---|---|---|---|---|---|---|
| | | | | | | | | | Class-conditional | | |
| | Return type | $f$ | Conifers | Mixed | Hardwoods | classes) | classified | Overall | Conifers | Mixed | Hardwoods |
| Normalized | Single | 2.042 | 65.3 (5.6) | 75.9 (8.5) | 86.2 (6.5) | 0.151 | 75.6 | 0.624 | 0.625 | 0.569 | 0.676 |
| | Single | 2.000 | 65.3 (5.5) | 76.0 (8.6) | 86.1 (6.6) | 0.152 | 73.3 | 0.593 | 0.700 | 0.476 | 0.598 |
| | 1st + single | 2.000 | 44.1 (8.4) | 53.8 (12.7) | 61.4 (9.8) | 0.271 | 57.8 | 0.361 | 0.444 | 0.297 | 0.330 |
| | 1st + single | 2.326 | 43.9 (8.1) | 53.5 (12.2) | 61.1 (8.9) | 0.259 | 62.2 | 0.426 | 0.519 | 0.318 | 0.442 |
| | 1st + single | 2.500 | 44.0 (8.3) | 53.7 (12.5) | 61.2 (9.2) | 0.263 | 60.0 | 0.394 | 0.444 | 0.351 | 0.378 |
| | 1st + single | 3.000 | 44.3 (9.5) | 54.0 (13.9) | 61.6 (10.0) | 0.284 | 53.3 | 0.291 | 0.298 | 0.243 | 0.330 |
| Observed | Single | - | 68.1 (20.5) | 78.0 (34.5) | 89.3 (27.5) | 0.338 | 44.4 | 0.165 | 0.192 | 0.123 | 0.184 |
| | 1st+Single | - | 47.9 (16.7) | 55.5 (26.6) | 62.3 (21.3) | 0.426 | 44.4 | 0.167 | 0.192 | 0.121 | 0.196 |

TABLE 3. Z SCORES PERTAINING TO PAIR-WISE COMPARISONS OF A THREE-CLASS LINEAR DISCRIMINANT ANALYSIS-BASED, CROSS-VALIDATION CLASSIFICATION OBTAINED BY USING ABOVE GROUND, SINGLE AND FIRST-OF-MANY LIDAR INTENSITY VALUES FROM 45 PLOTS

| Return type | a. | b. | c. | d. | e. | f. | g. |
|---|---|---|---|---|---|---|---|
| a. Observed, single | | | | | | | |
| b. Observed, 1st + single | 0.02 | | | | | | |
| c. Normalized ($f$ = 2.000), 1st + single | 1.73 | 1.72 | | | | | |
| d. Normalized ($f$ = 2.326), 1st + single | 2.33 | 2.32 | 0.61 | | | | |
| e. Normalized ($f$ = 2.500), 1st + single | 2.03 | 2.02 | 0.31 | −0.30 | | | |
| f. Normalized ($f$ = 3.000), 1st + single | 1.10 | 1.08 | −0.64 | −1.25 | −0.95 | | |
| g. Normalized ($f$ = 2.000), single | 3.99 | 3.99 | 2.28 | 1.66 | 1.96 | 2.93 | |
| h. Normalized ($f$ = 2.042), single | 4.32 | 4.32 | 2.61 | 1.98 | 2.29 | 3.26 | 0.33 |

Two-tail critical values at 10%, 5%, and 1% confidence level are 1.65, 1.96, and 2.56, respectively.
One-tail critical values at 10%, 5%, and 1% confidence level are 1.28, 1.65, and 2.32, respectively.

The intercept term in the second-order polynomial function that describes the relationship between $f$ and within-canopy range for above-ground return pairs shown in Figure 4, suggests some, albeit small, amount of attenuation in addition to the atmospheric rate to the very top of the canopy. The presence of an intercept appears to contradict the interpretation on pulse attenuation rates offered earlier. In previous work in the same area (Gatziolis *et al.*, 2010), however, it was determined that because the backscattering from the very top of the trees is usually weaker than the sensor's detection threshold, the highest-positioned returns from vegetation were located an average of 0.3 m for hardwoods at leaf-on conditions, and 0.6 for conifers below the actual tree tops. Adjusting the polynomial in Figure 4 to account for this discrepancy would reduce the value of the intercept to that computed using the laser data over the grass fields.

First-of-many returns are located in parts of the canopy where foliage and woody material of tree crowns are characterized by higher heterogeneity compared to the locus of single returns. They are also usually positioned lower in the canopy and are weaker, since enough energy in their parent pulses is preserved to generate more returns. In those conditions, the within-pair intensity differences are strongly influenced, if not dominated, by variable amounts of vegetation material intercepted by the pulse's footprint. As implied by studying Figure 3, increasing variability in observed intensities is interpreted in the normalization approach presented here as exclusively emerging from variability in range, which, in turn, causes artificial inflation of computed $f$ values. Since only a portion of the differences in observed intensity for first-of-many returns is actually range-related, the reduction in intensity CV before and after normalization is limited (Table 1).

Intensity differences in pairs of intermediate (subsequent to the first) returns are affected by the pulse discritization process, which is designed to provide a balanced representation of vegetation profiles at different height quantiles and of the ground surface. Their observed intensities are subject to pulse energy losses sustained at the locus of previous returns and the 3 m or 2 m portion of the trajectory following the previous returns. Reduced energy levels and longer within-canopy distances travelled by the parent pulses of first-of-many or intermediate returns increase the likelihood of multiple scattering effects, or path-reflectance as this phenomenon is sometimes known. These effects cause delays in the pulse response time, introduce non-linear range bias, and facilitate identification of paired returns that are not actually collocated. Considering that even for shade-tolerant species, such as bigleaf maple, foliage density is reduced with canopy depth, above-ground intermediate returns have a higher probability of representing energy backscattering from non-foliage, and therefore non-cover-type-related, material. The combination of low pulse energy availability, elevated probability for multiple scattering effects, and low probability for foliage presence within the pulses' footprint at the location of an intermediate return, leads to observed intensities with reduced cover-type-related information content and to proportionally large intensity differences in observed intensity within identified return pairs. Since these differences are mostly non-range-related, the benefit from using the normalization process toward classification accuracy improvements is marginal. Conversely, range normalization of single or first-of-many returns in laser acquisitions over forests characterized by steep slopes, or where the altitude of the airborne platform is variable, would likely improve the consistency of intensity measurements and benefit applications that utilize them. This inference is supported by the findings of the study by Korpela *et al.* (2010), where although kappa values of comparable magnitude to those computed in this study were obtained, the gains in classification accuracy contributed by the normalization process were marginal, likely because of limited range variability in their laser returns.

The normalization approach presented here can easily be adapted to modern lidar instruments that support dynamic adjustments in sensor gain, provided that the pulse-specific sensitivity is recorded and that the slope of the gain function is known (Korpela, 2008). The absence of prerequisites common in methods suggested elsewhere, for example the requirement for at least three distinct flight altitudes for a subset of the scanned area in the empirical method by Höfle and Pfeifer (2007), or the need for manual selection of reference targets by Korpela (2008), and the full automation potential indicates that the paired-return approach can be implemented as part of routine laser data preprocessing. Since observed and range-normalized lidar intensities are affected by a multitude of parameters, both intrinsic to the laser instrument and external, they should not be regarded as quantities surrogate to target, and for the purposes of this study, vegetation reflectance. A complete radiometric calibration of laser intensity would require information on the reflectance properties of selected targets present in the acquisition area. Determining target types that can serve as reliable backscattering references that can be used to convert intensity measurements to reflectance is an active field of research.

## Conclusions

Large range variability present in discrete-return, small footprint lidar data acquired over forests growing on steep

terrain reduces the consistency of observed intensity measurements and limits their ability to aid popular forest applications of laser data, including cover type classification. Attempts to normalize intensity data proportionally to the second power of the actual to mean (across all data) laser return range, was found to markedly improve the consistency of intensity data and therefore the accuracy of resulting cover type classifications. As demonstrated by this study, however, small additional consistency gains can be realized and classification accuracies can be further improved by deriving the value of the range-scaling exponent *f* dynamically from the data using an optimization process and by including in the normalization only above-ground, single returns. The novel approach for dynamic, largely automated, range-based intensity normalization introduced herein, is based on the data redundancy present in adjacent scanning swaths. The improved consistency of post-normalized data would likely benefit other applications that utilize lidar intensity measurements.

## Acknowledgments

The author would like to thank the Oregon Department of Forestry and the PNW Station Director's Office for funding support, and Watershed Sciences, Inc., of Corvallis, Oregon for the delivery of customized data products.

## References

Ahokas, E., S. Kaasalainen, J. Hyyppä, and J. Suomalainen, 2006. Calibration of the Optech ALTM 3100 laser scanner intensity data using brightness targets, *International Archives of Photogrammetry, Remote Sensing and Spatial Information Sciences*, 36(A1), CD-ROM.

Antonarakis, A.S., K.S. Richards, and J. Brasington, 2008. Object-based land cover classification using airborne LiDAR, *Remote Sensing of Environment*, 112(6):2988-2998.

Axelsson. P., 1999. Processing of laser scanner data - Algorithms and applications, *ISPRS Journal of Photogrammetry and Remote Sensing*, 54(2-3):138-147.

Brennan, R., and T.L. Webster, 2006. Object-oriented land cover classification of lidar-derived Surfaces, *Canadian Journal of Remote Sensing*, 32(2):162-172.

Chen, Q., 2007. Airborne lidar data processing and information extraction, *Photogrammetric Engineering & Remote Sensing*, 73(2):109-112.

Cohen, J., 1960. A coefficient of agreement for nominal scales, *Educational and Psychological Measurement*, 20:37-46.

Gatziolis, D., J.S. Fried, and V. Monleon, 2010. Challenges to estimating tree-height via LiDAR in closed-canopy forests: A parable from western Oregon, *Forest Science*, 56(2):139-155.

Goodwin, N.R., N.C. Coops, and D.S. Culvenor, 2006. Assessment of forest structure via airborne LiDAR and the effects of platform altitude, *Remote Sensing of Environment*, 103(2):140-152.

Höfle, B., and N. Pfeifer, 2007. Correction of laser scanning intensity data: Data and model-driven approaches, *ISPRS Journal of Photogrammetry and Remote Sensing*, 62(6):415-433.

Hopkinson, C., 2007. The influence of flying altitude, beam divergence, and pulse repetition frequency on laser pulse return intensity and canopy frequency distribution, *Canadian Journal of Remote Sensing*, 33(4):312-324.

Hopkinson, C., and L.E. Chasmer, 2009. Testing LiDAR models of fractional cover across multiple forest ecozones, *Remote Sensing of Environment*, 113(1):275-288.

Hudson, W.D., and C.W. Ramm, 1987. Correct formulation of the kappa coefficient of Agreement, *Photogrammetric Engineering & Remote Sensing*, 53(4):421-422.

Kaasalainen, S., J. Hyyppä, P. Litkey, H. Hyyppä, E. Ahokas, A. Kukko, and H. Kaartinen, 2007. Radiometric calibration of ALS intensity, *International Archives of Photogrammetry, Remote Sensing and Spatial Information Sciences*, 36(3/W52):201-205.

Kim, S., R.J. McGaughey, H.-E. Andersen, and G. Schreuder, 2009. Tree species differentiation using intensity data derived from leaf-on and leaf-off airborne laser scanner data, *Remote Sensing of Environment*, 113(8):1575-1586.

Korpela, I.S., 2008. Mapping of understory lichens with airborne discrete-return LiDAR data, *Remote Sensing of Environment*, 112(10):3891-3897.

Korpela, I.S., H.O. Ørka, J. Hyyppä, V. Heikkinen, and T. Tokola, 2010. Range and AGC normalization in airborne discrete-return LiDAR intensity data for forest canopies, *ISPRS Journal of Photogrammetry and Remote Sensing*, 64(4):369-379.

Luzum, B., M. Starek, and K.C. Slatton, 2004. Normalizing ALSM intensities, *Geosensing Engineering and Mapping (GEM) Center Report No. Rep_2004_07_001*, URL: *http://www.aspl.ece.ufl.edu/reports/GEM_Rep_2004_07_001.pdf*, Civil and Coastal Engineering Department, University of Florida (last date accessed: 15 December 2010)

Press, W.H., S. Teukolsky, W. Vetterling, and B. Flannery, 2002. *Numerical Recipes in C, The Art of Scientific Computing*, Cambridge University Press, 401 p.

Rosenfield, G.H., and K. Fitzpatrick-Lins, 1986. A coefficient of agreement as a measure of thematic classification accuracy, *Photogrammetric Engineering & Remote Sensing*, 52(2):223-227.

Venables, W.N., and B.D. Ripley, 2002. *Modern Applied Statistics with S*, Fourth edition, Springer, New York, 496 p.

Vosselman, G., 2000. Slope based filtering of laser altimetry, *International Archives of Photogrammetry and Remote Sensing*, 33(B3/2):935-942.

Wagner, W., A. Ullrich, V. Ducic, T. Melzer, and N. Studnicka, 2006. Gaussian decomposition and calibration of a novel small-footprint full-waveform digitizing airborne laser scanner, *ISPRS Journal of Photogrammetry and Remote Sensing*, 60(2):100-112.